iScience

CellPress
OPEN ACCESS

Article

Discovery of an unrecognized nidovirus associated with granulomatous hepatitis in rainbow trout

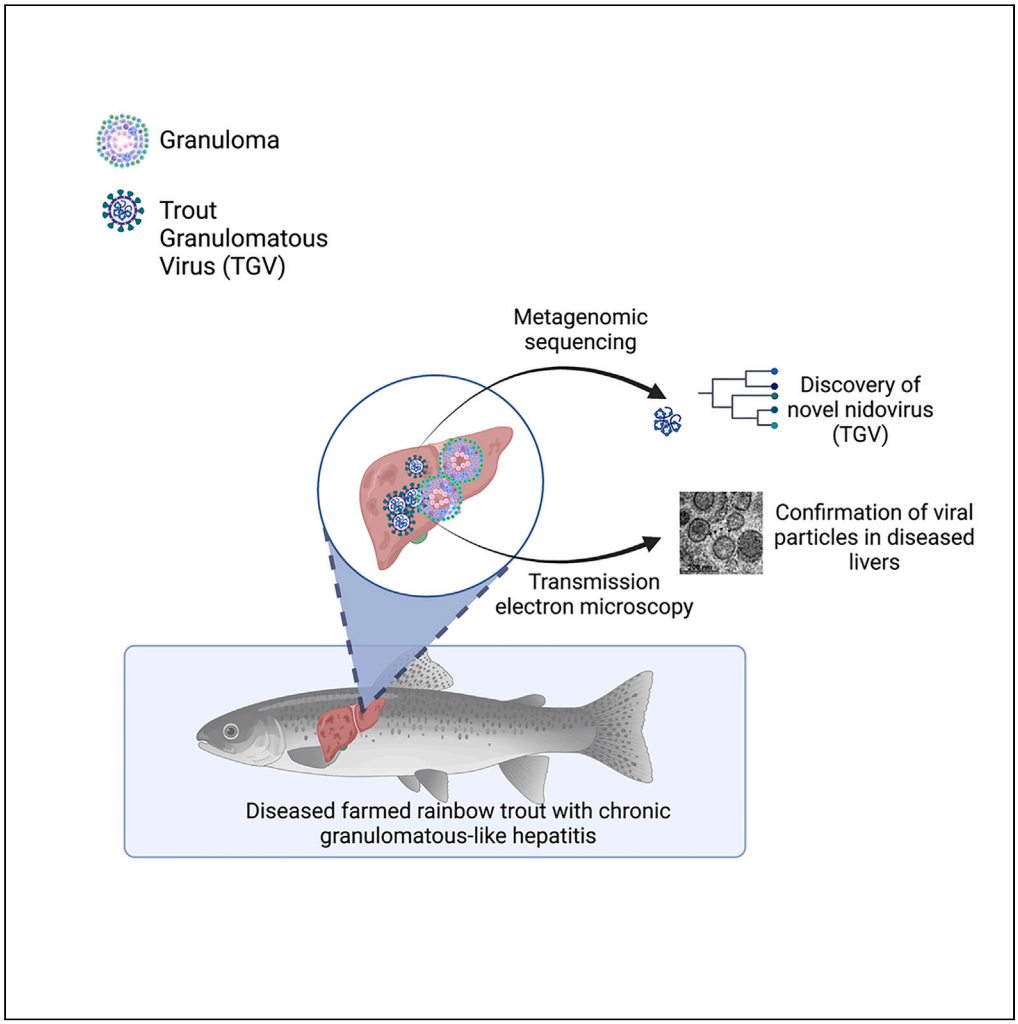

Sharon Karniely, Adi Faigenboim, Salsabeel Watted, ..., Asaf Berkowitz, Eran Bacharach, Avi Eldar

sharonk@moag.gov.il (S.K.)
eranba@tauex.tau.ac.il (E.B.)
eldar@moag.gov.il (A.E.)

Highlights

A new disease diagnosed in rainbow trout characterized by granulomatous hepatitis

Electron microscopy revealed coronavirus-like particles in liver lesions

High-throughput sequencing revealed a novel piscine nidovirus in affected livers

Transcripts of the novel virus are abundant in internal organs of diseased trout

Karniely et al., iScience 26, 106370
April 21, 2023
https://doi.org/10.1016/j.isci.2023.106370

iScience

CellPress
OPEN ACCESS

Article

Discovery of an unrecognized nidovirus associated with granulomatous hepatitis in rainbow trout

Sharon Karniely,[1,8,10,*] Adi Faigenboim,[2,8] Salsabeel Watted,[1] Katia Lapin,[1] Eduard Berenshtein,[3] Avshalom Hurvitz,[4] Arieli Bouznach,[1] Ezra Rozenblut,[1,9] Massimo Orioles,[5] Marco Galeotti,[5] Irene Salinas,[6] Asaf Berkowitz,[1] Eran Bacharach,[7,*] and Avi Eldar[1,*]

SUMMARY

Rainbow trout (*Oncorhynchus mykiss*) is the principal species of inland-farmed fish in the Western hemisphere. Recently, we diagnosed in farmed rainbow trout a disease in which the hallmark is granulomatous-like hepatitis. No biotic agents could be isolated from lesions. Still, unbiased high-throughput sequencing and bioinformatics analyses revealed the presence of a novel piscine nidovirus that we named "Trout Granulomatous Virus" (TGV). TGV genome (28,767 nucleotides long) is predicted to encode non-structural (1a and 1 ab) and structural (S, M, and N) proteins that resemble proteins of other known piscine nidoviruses. High loads of TGV transcripts were detected by quantitative RT-PCR in diseased fish and visualized in hepatic granulomatous sites by fluorescence *in situ* hybridization. Transmission electron microscopy (TEM) revealed coronavirus-like particles in these lesions. Together, these analyses corroborated the association of TGV with the lesions. The identification and detection of TGV provide means to control TGV spread in trout populations.

INTRODUCTION

Rainbow trout *Oncorhynchus mykiss* (Walbaum) is a North Pacific salmonid species, which, in the Western hemisphere, is the principal inland-farmed fish. In terms of production, global rainbow trout reached 600,000 tons in 2012, and by 2019 it had exceeded 950,000 tons (http://www.fao.org/tempref/FI/DOCUMENT/aquaculture/CulturedSpecies/file/en/en_rainbowtrout.htm). Increased production incited the intensification of aquaculture systems; modern recirculating systems replaced traditional ponds, and family-run farms were assimilated by large industrial corporations.[1] The outcome of these changes (intensive aquaculture) is the rearing of high densities of animals in limited space (closed environment). This outcome, combined with the increased trafficking of stocks between farms (globalization), has instigated the emergence and spread of infectious diseases (mechanical transmission). Rainbow trout sleeping disease (caused by alphavirus) and piscine reovirus 3 (orthoreovirus)-associated disease are examples of emerging viral diseases that have widely spread and turned into significant threats to the sustainability of trout farming.[2,3] Infectious hematopoietic necrosis virus (IHNV) and viral hemorrhagic septicemia virus (VHSV), both of the family *Rhabdoviridae* identified decades ago,[4,5] remain a threat to rainbow trout as well as other salmonids. Complex environments of fish farms located in large geographical areas have also contributed to the spread of diseases through currents that are capable of moving pathogens over many tenths of kilometers (waterborne transmission), as shown by the salmon pancreatic disease (caused by the Salmonid alphavirus) and the infectious salmon anemia (caused by the Salmon isavirus).[6–9]

Here we describe a novel and ongoing disease in farmed rainbow trout, in which the hallmark consists of hepatic granulomatous-like lesions. No biotic agent could be cultured from the diseased fish. Still, unbiased high-throughput sequencing and bioinformatics analyses enabled us to identify and assemble the complete genome sequence of a novel nidovirus (28,767 nucleotides long), phylogenetically belonging to the Piscanivirinae subfamily. The viral RNA load, tissue distribution, and spatial localization corroborate an association between the new virus and the described disease.

[1]Department of Virology, Kimron Veterinary Institute, Bet Dagan 50250, Israel

[2]Department of Plant Pathology, The Volcani Center, Bet Dagan 50250, Israel

[3]EM Unit Research Core Facility at Hebrew University of Jerusalem – Hadassah Medical School, Jerusalem, Israel

[4]Dan Fish Farm, Kibbutz Dan, Upper Galilee, Israel

[5]Veterinary Pathology Unit, Department of Agricultural, Food, Environmental and Animal Sciences, University of Udine, Udine, Italy

[6]Department of Biology, University of New Mexico, Albuquerque, NM 87131-0001, USA

[7]The Shmunis School of Biomedicine and Cancer Research, The George S. Wise Faculty of Life Sciences, Tel Aviv University, Tel-Aviv 69012, Israel

[8]These authors contributed equally

[9]RIP

[10]Lead contact

*Correspondence: sharonk@moag.gov.il (S.K.), eranba@tauex.tau.ac.il (E.B.), eldar@moag.gov.il (A.E.)

https://doi.org/10.1016/j.isci.2023.106370

The discovery of a novel virus among diseased fish is the initial step in pathogen identification and disease control.

RESULTS

An outbreak of hepatic granulomatosis disease in farmed rainbow trout

In 2018, while conducting a routine postmortem diagnostic examination of farmed rainbow trout raised in Northern Israel, we revealed fish exhibiting protruding nodular masses restricted to the livers. These were white tan, raised, and rough and appeared at various extents. Similar previous years' examinations detected no affected fish despite a large number of fish examined yearly (700–1200). We concluded that this is likely a recent outbreak of a disease. The following year (and until the present), we recorded additional cases involving two more farms that share common water resources with the previous. Heightened surveillance alluded to an enduring disorder that comprised 4%–7% of the total population of fish weighing over 250 g each (on-growing and fattening stages). The hepatic lesions consisted of multiple small miliary nodular lesions, large and solid foci, and diffused fibrosis with simultaneous nodular regeneration (detailed below). Routine laboratory practices, Office International des Epizooties (OIE)-based procedures, and staining procedures (STAR Methods) failed to reveal known parasites, bacteria, viruses, or toxins/aflatoxins.

Affected fish were ill thrift, had stunted growth, and gathered at the end of the raceway. Compared to healthy fish, diseased fish were less responsive to external stimuli (sluggishness) and showed diminished food consumption (reduced appetite). These are non-pathognomic signs suggestive of general weakness. Although cumulative die-offs were relatively contained, economic losses due to poor feed conversion ratio, delayed growth, and condemnation of stocks (by the veterinary authorities) were substantial, especially as the disease was evident at relatively advanced stages of growth (250–450 gr).

Disease characteristics: Gross and microscopical findings

Examination of the clinically diseased fish revealed that gill pallor was the most prominent external hallmark (31 out of 50), suggesting anemia of chronic disease. We recorded skin hyperpigmentation in 6 of 50 examined fish and jaundice in a single case. Postmortem examination revealed enlarged livers in diseased fish (Figures 1A–1D) compared to healthy fish (Figure 1E). The extent of the enlargement varied from mildly to markedly enlarged, according to the severity of the lesions. The livers contained multifocal protruding, nodular masses, covering less than 10% of the hepatic parenchyma in early stages (Figure 1A), coalescing and replacing up to 50% of the parenchyma in subacute lesions (Figure 1B), and replacing the entire normal parenchyma along with fibrosis and acquired portosystemic shunts in the advanced chronic stage (Figures 1C and 1D). The masses were roughly spherical, slightly firm, white tan, homogeneous on cut section, and varying in size between 2 and 30 mm. There was a distended abdomen in 29 of the 50 fish, and the celomic cavity contained moderate to large amounts of clear fluid (ascites) or blood (Figures 1C and 1D).

Microscopically, the hepatic lesions were roughly grouped into four stages: acute inflammation with mild tissue injury, subacute inflammation with moderate damage, subacute-to-chronic stage with marked effacement of the normal parenchyma, and chronic to chronic-active hepatitis (the latter exhibiting the most severe and irreversible lesions). Within the livers of the first group (acute disease), the hepatic parenchyma is multifocally and randomly expanded by large aggregates of vacuolated histiocytes and scattered multinucleated giant cells, often surrounded by a thin outer rim of small numbers of lymphocytes (granulomatous-like reaction) (Figure 2A). Occasionally within the granulomatous-like reaction, there were foci of necrosis and karyorrhectic debris as well as some histiocytic cells. Often, large blood vessels were congested and cuffed by small aggregates of lymphocytes (Figure 2A). The adjacent hepatic parenchyma retained its normal architecture. In the second group (subacute disease), there were large amounts of vacuolated histiocytes, surrounded by a prominent thick layer of large numbers of lymphocytes (Figure 2B). The lymphocytic cuffings around blood vessels were large and formed aggregates. However, the remaining parenchyma of the liver still maintained a typical architecture. The third group, characterized by subacute to early chronic disease, exhibited smaller aggregates of macrophages and histiocytes with a paucity of vacuolar contents and large numbers of lymphocytes, occasionally forming coalescing sheets admixed with large numbers of reactive young fibroblasts alongside small depositions of immature collagen fibers (Figure 2C). The fibroblasts expanded and infiltrated the adjacent hepatic parenchyma and disrupted its normal architecture by separating and destroying the lobular pattern. The fourth group, characterized by a late chronic to a chronic-active stage of the disease, exhibited the most severe lesions correlated

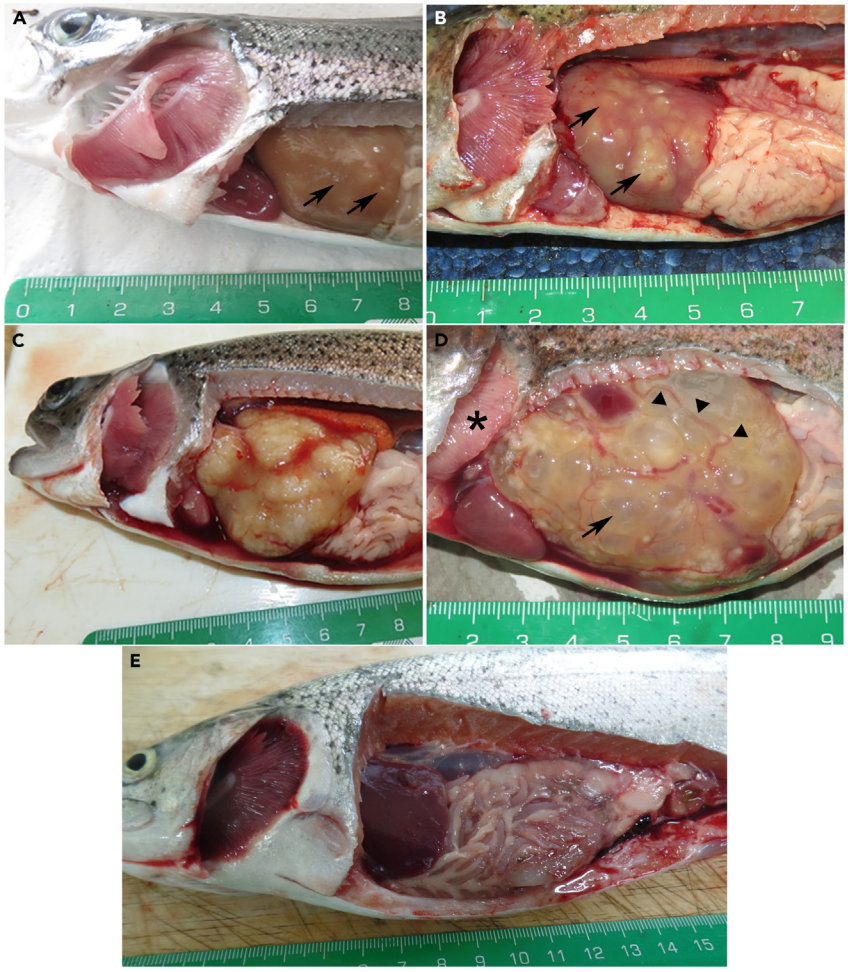

Figure 1. Gross pathology of diseased Rainbow trout

(A) Early-stage lesions. The hepatic parenchyma is mottled with small 1-3 mm in diameter, white, tan discrete nodules (arrows). The nodules replace less than 10% of the hepatic parenchyma.

(B) Moderately affected liver. Lesions consist of multiple white tan, slightly elevated masses, ranging between 2 and 10 mm in diameter (arrows), affecting approximately 50% of the hepatic parenchyma. The latter retains normal architecture between the masses.

(C) Markedly affected liver. Large white masses coalesce at the liver's ventral aspect and replace 70-80% of the normal hepatic parenchyma.

(D) Severely affected liver. Severe liver fibrosis. White, tan masses mottled with multifocal transparent cysts (arrow) efface the entire parenchyma. Multiple tortuous blood vessels (arrowheads) outline the capsule. These are, likely, acquired portosystemic (portal vein to hepatic vein) shunts, consistent with increased resistance to the portal flow within the liver (due to the severe fibrosis). The gills are pale, suggesting anemia of chronic disease (asterisk).

(E) Normal liver in a healthy rainbow trout.

with the severe extrahepatic lesions of ascites, acquired portosystemic vascular shunts, and rarely post-hepatic obstruction and jaundice. The entire hepatic parenchyma was distorted: its majority was replaced by thick bands of mature collagen, gradually replacing the fibroplasia (Figure 2D). The deposition of collagen dissected the hepatic lobules, destroying the lobular limiting plates, forming small islets of hepatocytes along with marked bile duct and arteriolar hyperplasia. There were still large aggregates of lymphocytes and small multifocal clusters of histiocytes and necrotic centers (chronic-active inflammation). The capsular surface was corrugated ("lumpy-bumpy") and covered by fibrosis. Small numbers of lymphocytes and neutrophils were admixed with fewer fibrocytes and scattered small-to-moderate numbers of lymphocytes and hypertrophic mesothelial cells. There was a proliferation of small blood vessels on the capsule (portosystemic shunts) (Figure 2D).

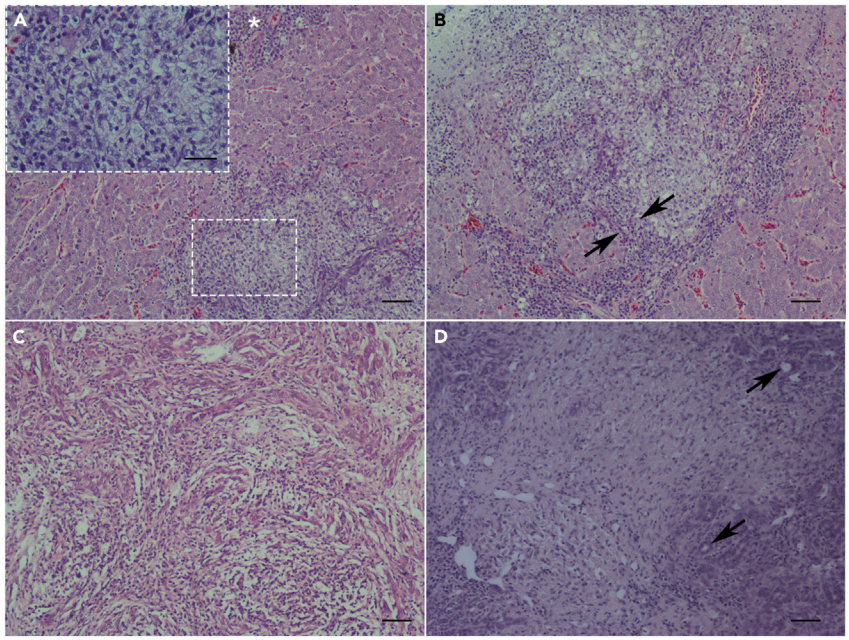

Figure 2. Histopathological findings in livers of diseased Rainbow trout

(A) An early (acute) stage of granulomatous inflammation with large numbers of foamy macrophages (view inset) surrounded by small numbers of lymphocytes. The enlarged inset (H&E X 400) displays a large number of vacuolated histiocytes infiltrating the liver. The hepatic parenchyma adjacent to the lesions retains normal architecture (H&E X 100). There are very few to no lymphocytes surrounding the histiocytes, but adjacent to blood vessels there are larger aggregates of lymphocytes (asterisk).

(B) Acute to subacute stage. A large aggregate of vacuolated histiocytes surrounded by a prominent rim of lymphocytes (subtended by arrows). The adjacent parenchyma is normal (H&E X 100).

(C) Subacute to chronic stage of inflammation. Large numbers of lymphocytes are observed, alongside robust fibroplasia, replacing most of the histiocytes (H&E X 100).

(D) Late stage (chronic) of inflammation. Most of the inflammatory infiltrate is replaced by broad bands of mature fibrosis with paucity of inflammatory cells and fibrocytes (mature collagen) dissecting and distorting islets of remnants of hepatic parenchyma, alongside marked bile ducts hyperplasia (arrows) (H&E X 100). Bars: A-D = 100 μm, A inset = 50 μm.

Identification of coronavirus-like particles in livers of diseased fish

Necroscopic, parasitological, and bacteriological/mycological examinations of liver tissues from diseased fish failed to reveal known parasites, bacteria, fungi, or toxins/aflatoxins. Although rare, there are reports of viral (coronavirus) infections associated with a granulomatous reaction in domestic cats, other felids, and ferrets.[10,11] In conjunction with the absence of any known biotic agents associated with the reported lesions, these led us to explore the presence of viruses in affected livers. To visualize possible viruses, we examined by transmission electron microscopy (TEM) two samples with moderate to severe diffuse granulomatous hepatitis. Thin section analysis revealed the presence of sparse and roughly spherical electron-dense particles within the cytoplasm of hepatocytes in both fish. These particles were enveloped and measured 90–100 nm in diameter. Characteristic coronavirus-like (15–20 nm) club-shaped projections (spikes) were observed on their surfaces (Figure 3).

Attempts to isolate the virus through culturing in multiple established piscine cell lines and rainbow trout primary cells have failed: viral RNA was detectable by RT-PCR (see below) in the inoculums but disappeared from culture supernatants upon media replacement and culture passages. In addition, we did not observe any cytopathic effects in inoculated cultures. Thus, we applied molecular approaches to identify the virus that we detected by TEM in the livers of diseased fish.

High-throughput sequencing reveals sequences of a novel nidovirus in affected livers

We performed metagenomic analyses of rRNA-depleted RNAs extracted from diseased and healthy fish liver samples. Ilumina sequencing yielded 12.4 M and 11.2 M of 2 × 150 -nucleotide paired-end reads. We first mapped the reads to the rainbow trout reference genome and then used the unaligned reads as a query term for a

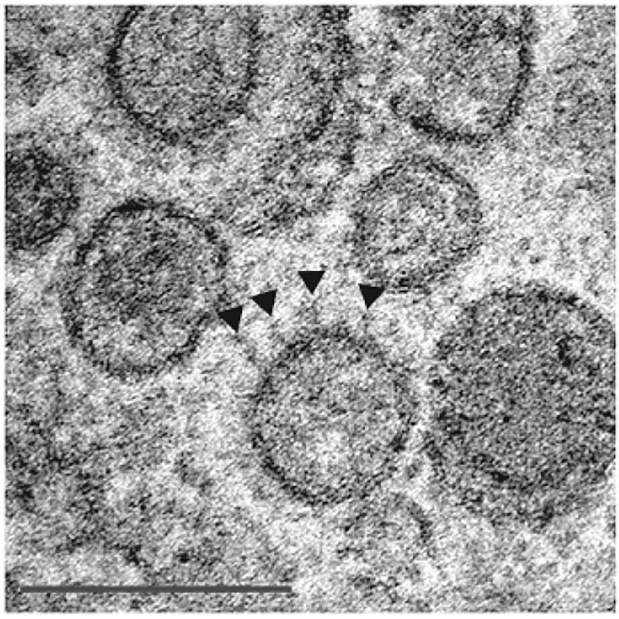

Figure 3. Coronavirus-like particles observed in livers of diseased fish

Transmission electron microscopy (TEM) micrograph of a fixed, thin section of liver biopsy from diseased trout. Arrowheads point to spike-like projections decorating the virion surface. Bar = 200 nm.

search in the National Center for Biotechnology Information (NCBI) non-redundant (nr) protein database. Reads were taxonomically classified using the NCBI nucleotide database. This search enabled us to detect 15 reads unique to the diseased-fish sample, having predicted amino acid (aa) sequences with homology (46%–67% pairwise aa identity) to sequences within the replicase polypeptide pp1ab of two piscine nidoviruses: the fathead minnow nidovirus (FHMNV; Genbank:YP_009505581[12]) and the white bream virus (WBV; Genbank:YP_803213[13]). We designed primers derived from these unique reads, which allowed the amplification of sequences that reside in the gaps between the reads (by RT-PCR, using RNA from diseased fish as a template, Figure 4B and Table S1). We assembled the amplified sequences using the Genious 9.1.8 software (https://www.geneious.com) and analyzed the resulting assemblies with BlastX and the GenBank nr protein sequences database. This procedure identified a 6,157 base-long transcript of an uninterrupted open reading frame (ORF). The predicted translation product of this transcript shares homology (~45% identity and ~60% similarity) to the polyprotein 1 ab of three bafiniviruses—Chinook salmon bafinivirus (CSBV), FHMNV, and WBV. Guided by this homology, we identified in the newly discovered ORF1b sequences potentially encoding for RNA-dependent RNA polymerase (RdRp), HEL1 (superfamily 1 helicase), 3′-to-5′ exonuclease (ExoN), nidoviral endoribonuclease specific for U (NendoU), and S-adenosylmethionine-dependent ribose 2′-*O*-methyltransferase (OMT; Figure 4B). Of note, the organization of these ORFs is typical of members of the nidovirales order. The RdRp and helicase proteins are relatively conserved among nidoviruses and serve for phylogeny.[14,15] The phylogenetic analysis (Mafft tool; https://mafft.cbrc.jp/alignment/server/,[16]) based on the RdRp (Figure 4C) and helicase (Figure S1) aa sequences confirmed that the newly identified virus is related to nidoviruses of the tobaniviridae family and *piscanivirinae* subfamily, which includes CSBV and Atlantic salmon bafinivirus (ASBV) of the *oncotshavirus* genus and FHMNV and WBV of the *bafinivirus* genus.[17]

Hence, the TEM data coupled with the sequence analyses demonstrate that the lesions contain a previously unknown virus, a member of the order *Nidovirales*. To reference the peculiar pathogenic hallmark of the infection by the newly identified virus, we provisionally named this putative disease-causing agent "Trout Granulomatous Virus" (TGV).

RT-PCR and fluorescence *in situ* hybridization (FISH) assays confirm the association of TGV with the disease

To further explore the possible linkage between TGV and hepatic disease, we established an RT-PCR assay for detecting TGV viral RNA. To this end, total RNA was extracted from livers and subjected to RT-PCR

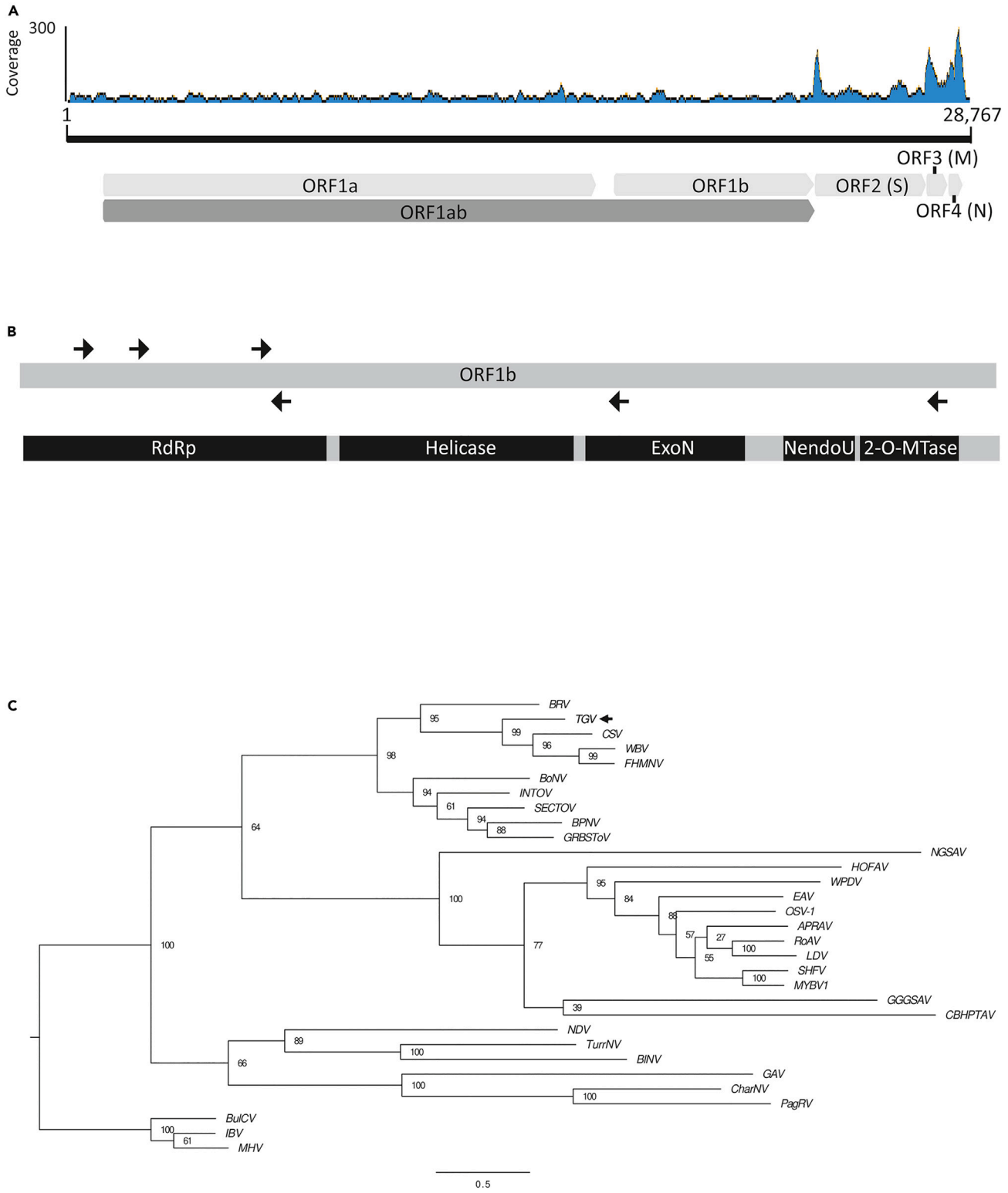

Figure 4. Schematic representation of the TGV genome, predicted domain organization of TGV ORF1b, and phylogenetic analysis

(A) Illustration of the TGV genome. Major ORFs are marked by arrows, and corresponding predicted polypeptides are indicated in brackets. RNA-seq reads coverage across the genome is shown above.

Figure 4. *Continued*

(B) Schematic presentation of ORF1b with the location of primers used for PCR amplification (top, arrows) and domain prediction (bottom) of the identified 1b polypeptide, based on homology to the WBV replicase.

(C) Phylogenetic tree, based on the predicted aa of RdRp, generated with the Phyml software, based on maximum likelihood method.[18] Arrows mark TGV locations in the trees. TGV sequences (Genbank: NM_OM397548) were compared to sequences of representative species of known genera within the *Niodvirales* order. These representatives included the Bovine torovirus (BRV, Genbank: NC_007447), Chinook salmon bafinivirus (CSV, Genbank: NC_026812), White bream virus (WBV, Genbank: NC_008516), Fathead minnow nidovirus (FHMNV, Genbank: NC_038295), Bovine nidovirus (BoNV, Genbank: NC_027199), Infratovirus (INTOV, Genbank: NC_033700), Sectovirus (SECTOV, Genbank: NC_043490), Ball python nidovirus (BPNV, Genbank: NC_024709), Guangdong red-banded snake-*Lycodon rufozonatus*-torovirus (GRBSToV, Genbank: NC_046963), Nanhai ghost shark arterivirus (NGSAV, Genbank: NC_046960), Hainan oligodon formosanus arterivirus (HOFAV, Genbank: NC_046958), Wobbly possum disease virus (WPDV, Genbank: NC_026811), Equine arteritis virus (EAV, Genbank: NC_002532), Olivier's shrew virus 1 (OSV-1, Genbank: NC_035127), Lactate dehydrogenase-elevating virus (LDV, Genbank: NC_001639), Rodent arterivirus (RoAV, Genbank: NC_KY369969), African pouched rat arterivirus (APRAV, Genbank: NC_026439), Simian hemorrhagic fever virus (SHFV, Genbank: NC_003092), Mikumi yellow baboon virus 1 (MYBV1, Genbank: NC_025112), Guangdong greater green snake arterivirus (GGGSAV, Genbank: NC_046959), Chinese broad-headed pond turtle arterivirus (CBHPTAV, Genbank: NC_046961), Nam Dinh virus (NDV, Genbank: NC_015874), Turrinivirus 1 (TurrNV, Genbank: NC_032496), *Botrylloides leachii* nidovirus (BlNV, Genbank: NC_MK956105), Gill-associated virus (GAV, Genbank: NC_010306), Charybnivirus 1 (CharNV, Genbank: NC_032492), Paguronivirus 1 (PagRV, Genbank: NC_032490), murine hepatitis virus (MHV, Genbank: NC_048217), Bulbul coronavirus HKU11 (BulCV_HKU1, Genbank: NC_011547), and Infectious bronchitis virus (IBV, Genbank: NC_001451). The alignment was performed by MAFFT program [http://mafft.cbrc.jp/alignment/server/version,[16]]. Bar, 0.5 substitutions per amino acid position. See also Figure S1.

reactions using TGV-specific primers (Table S1). The amplified product of this assay showed the expected size (1 kb), was generated only after the reverse-transcription step and was sensitive to pre-treatment with RNase A (but not with DNase I) (Figure S2). Sanger sequencing of the amplified fragment confirmed its ORF1b TGV origin. These results demonstrated that TGV has an RNA genome. Using this assay, we detected TGV sequences in 43 samples of clinically diseased fish and 3 fish with no apparent macroscopic lesions. In addition, 3 local (Israeli) fish with no apparent disease signs (belonging to the control group) were positive for TGV, while all foreign (Italian) control fish scored negative (data not shown).

To investigate the spatial localization of TGV RNA, we applied *in situ* hybridization technique to liver samples of diseased fish, using TGV-derived, Quasar 570-conjugated, Stellaris FISH probes (Table S2). Following hybridization, we detected viral RNA-specific signals in the cytoplasm of hepatocytes. These hepatocytes clustered mainly in confined foci, which mapped to the granulomatous lesions (Figures 5 and S3). These results further demonstrate the association between TGV and the hepatic disease.

TGV transcripts in viscera of diseased and healthy fish

Granulomatous-like hepatitis is the most discernable pathology found in TGV-diseased fish. Indeed, TGV RNA was readily detected in these lesions (~16,000 copies/mg wet tissue, using synthetic RNA as a reference; STAR Methods). Because the virus may reside in additional organs, we next determined the presence of TGV transcripts in the livers, kidneys, spleens, and hearts. Samples were collected from 14 diseased fish and 14 apparently healthy fish and analyzed by RT-qPCR assay with TGV-derived primers and a probe (Table S1, Figure 6). In the liver of sick fish, the median $\log_{10}$ relative TGV abundance (normalized to host 18S rRNA transcript) peaked at 3.7. In the same diseased fish, we found a similar relative abundance of TGV transcripts in hearts ($\log_{10}$ ratio = 3.7) and spleens ($\log_{10}$ ratio = 3.3). TGV transcripts were significantly less abundant (p value = 0.004) in the kidneys ($\log_{10}$ ration = 2.2). No gross pathologies were observed in organs other than the liver. Altogether, TGV can be detected in the liver, heart, spleen, and kidney, but the apparent pathology is restricted to the liver. In the (apparently) healthy group, the relative normalized TGV median log values were 0.0, 0.4, 0.9, and 0.7 for the liver, kidney, spleen, and heart, respectively (Figure 6). Of note, positivity among apparently healthy individuals from the same diseased farm was also documented for other viruses and diseases (see discussion).

TGV complete genome shows similar domain organization to known piscine nidoviruses with unusually long ORF1a

To reveal the entire sequence of TGV genome, we combined RNA sequencing (RNA-seq) (30 million 2x150 paired-end reads obtained from a liver sample pre-screened for the high abundance of TGV-specific replicase sequences), complemented with 3′ rapid amplification of cDNA ends (3′ RACE), and RT-PCR of gapped regions. These procedures enabled us to assemble the complete genome of TGV (GenBank:NC_OP060531; Figure 4A), consisting of 28,767 nucleotides and four major ORFs. ORF1 contained the two large canonical 5′ ORFs: ORF1a and ORF1b. The predicted polyprotein pp1a (5,256 aa) is significantly larger than the corresponding polypeptides of WBV (4,555 aa), FHMNV (4,860 aa), and

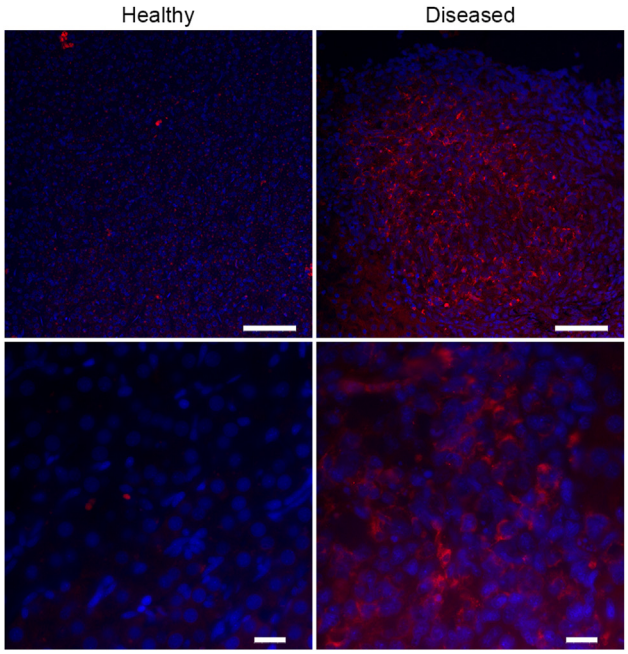

Figure 5. Detection of TGV RNA in rainbow trout livers by FISH

Low (upper panel) and high (lower panel) magnifications of sections of livers from healthy and diseased fish; the latter exhibit granulomas. The sections were hybridized with Quasar 570-conjugated, TGV-derived Stellaris RNA FISH probes (red) and counterstained with Hoechst dye (blue). Bars: upper panels = 100 μm, lower panels = 20 μm. See also Figure S3.

CSBV (4,685 aa). Of note, the sequence of the first 2,180 aa of TGV 1a shows no significant homology to any deposited protein sequence in the NCBI nr database (analyzed by BlastP). Residues 4,086-4,263 of TGV 1a show homology to the WBV Mpro 3C-like protease (31% identity, 50% similarity), including three conserved residues essential for WBV Mpro catalytic activity (Ser-3589/4226, His-3492/4134, and Asp-3518/4159, in WBV and TGV, respectively[19]). Akin to WBV, the Mpro homologous domain of TGV is flanked by predicted transmembrane (TM) domains.[13,19] In addition, NCBI conserved domains algorithm[20] revealed that TGV 1a contains areas with homology to coronavirus Nsp3 (TGV1a, aa 2351–2480), coronavirus Nsp8 (TGV1a, aa 4914- 5060), and deltacoronavirus Nsp10 (TGV1a, aa 5187-5240).

Nidoviruses express polyproteins pp1a and pp1ab from ORF1a and ORF1b, where synthesis of pp1ab depends on −1 ribosomal frameshifting, which occurs at a heptanucleotide "slippery sequence" (UUUAAAC).[21] Indeed, all coronaviruses, bafiniviruses, and toroviruses share this sequence. We identified the same heptanucleotide in the overlap between ORF1a and ORF1b, suggesting that TGV pp1ab translation may also involve a −1 ribosomal frameshifting.

ORF2 encodes a predicted 1,179 aa-long polypeptide, likely the spike (S) protein. We based this notion on the location of ORF2 in a genomic region that typically encodes the S protein in nidoviruses. Moreover, the domain organization of the protein resembles the one of a typical nidovirus S protein—a cleavable signal peptide at the N terminus, followed by the S1 receptor-binding domain and the S2 domain that mediates fusion with the host lipid membrane. Indeed, the first 21 aa of the predicted protein show a high probability (0.98) of serving as a signal peptide (inferred by SignalP 6.0[21,22]), where the N-terminal half of this protein shows significant homology to FHMNV S protein (38% identity, 54% similarity), including a conserved domain of type II chitinases (aa: 200- 450).[12] The C-terminal half contains regions of homology with predicted S proteins of piscine nidoviruses and toroviruses. A single TM domain close to the C-terminal end (aa 1167-1179) was predicted using the TMHMM 2.0 algorithm.[23,24]

TGV ORF3 encodes a predicted polypeptide of 222 aa. Three TM helices were predicted using the TMHMM 2.0 algorithm[23,24] within the first half of ORF3 (aa: 37-59, 66-88, and 101-123), similar to WBV ORF3,[13] FHMNV, and CSBV, and typical to the M protein of different nidoviruses.[25] Within the first 170 aa, TGV ORF 3 translated sequence shares 42%–48% similarity with predicted M proteins in the other piscine nidoviruses.

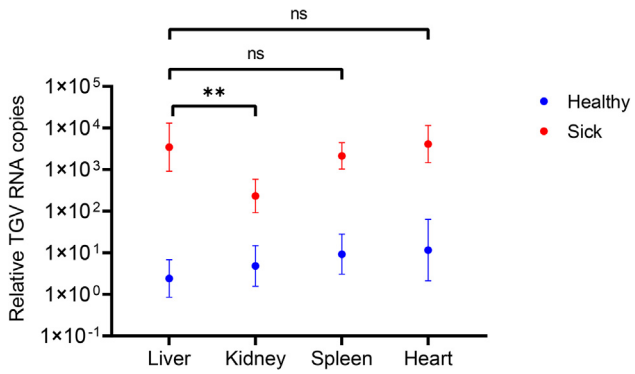

Figure 6. Relative abundance of TGV RNA in internal organs of sick and healthy rainbow trout

The relative abundance of TGV transcripts in the liver, kidney, spleen, and heart tissues of healthy and diseased fish is presented. Values represent the geometric mean values with confidence interval (CI) from n = 14 healthy and n = 14 sick fish. Pairwise analysis of significance of differences between liver and other tissues from sick fish (as denoted by horizontal lines) was performed using Mann-Whitney U test. **p < 0.01; ns, not significant.

The fourth nonoverlapping ORF of TGV encodes a predicted polypeptide of 148 aa, which resembles the nucleoproteins (N) of WBV, FHMNV, and CSBV (42%, 49%, and 36% similarity, respectively). The calculated isoelectric point (pI) for all these N proteins is high (9.94 for TGV N) and is characteristic of RNA-binding proteins.

Detection of TGV sub-genomic transcripts in infected fish tissues

A hallmark of Nidovirus replication is the production of nested co-terminal viral sub-genomic transcripts, which encode structural and accessory proteins.[26] For coronaviruses and arteriviruses, the sub-genomic transcripts contain a 5′ end leader sequence (65-98 bases), with identity to the 5′ end of the genomic RNA. A leader sequence of 42 nucleotides was found in the three sub-genomic transcripts of WBV.[13] To identify a potential sub-genomic leader sequence for TGV, we mapped reads in our RNA-seq data (from TGV-positive tissue) to the coding sequences (CDSs) of the predicted S, M, and N proteins. Aligned reads were divided into two groups, one showing complete identity with the genomic sequence upstream of the CDS, while the other group contained reads with 5′ sequences identical to the 5′ end of the assembled TGV genome. Alignment of the reads of the latter group revealed a 23 base sequence (CACAAA CACUAUUUCAAAACUGC) identical between the 5′ end genomic sequence and S and M reads, while the first two bases (CA) were not found in N-specific reads.

To explore if this 23 nucleotides sequence represents a leader sequence, we designed a forward leader-specific primer and matching reverse primers ca 400-700 bases downstream of the 5′ end of the genome and the predicted initiating codon AUG of S, M, and N CDSs (Table S1). RT-PCR performed with these primer sets produced amplicons of the expected sizes for RNA extracted from TGV-infected (S) but not from control (C) fish tissues (Figure S4). Of note, RT-PCR with the N reverse primer amplified two amplicons; the size of the smaller (500 bp) is in line with an N sub-genomic transcript while the larger (>1200 bp) is consistent with a sub-genomic transcript including both M and N sequences. The higher abundance of the 500 bp amplicon likely reflects the higher abundance of N-specific reads in our RNA-seq data (Figure 4A) and is consistent with the high abundance of N sub-genomic transcripts in other nidoviruses.[13] Cloning and Sanger sequencing of the amplicons confirmed the presence of the expected genomic sequence or structural protein CDS downstream of the leader sequence. We found no evidence for additional transcripts containing a leader sequence preceding internal or overlapping ORFs predicted in the TGV genome.

DISCUSSION

This study describes a new disease in rainbow trout characterized by hepatic granulomatosis. Our histopathological, molecular, and phylogenetic analyses, supported by *in situ* hybridization studies, indicate that the hepatic disease in rainbow trout is associated with a novel nidovirus related to, but distinct from, previously described piscine bafiniviruses.

As a newly discovered virus, fundamental questions related to the biology of this pathogen, its associated disease, and the modalities of transmission are essentially unknown. Foremost is whether this virus causes the observed disease and hepatic pathology. It is not always attainable to establish a causative relationship between a pathogen and its related disease in a host by fulfilling Koch's postulates. Ethical issues, availability of adequate experimental models, or lack of culture methods hamper the reproduction of experimental disease. The case of HIV and acquired immunodeficiency syndrome (AIDS) is perhaps the archetypical example, where the disease was described before the virus was successfully cultured,[27] and recapitulation of immunodeficiency in animal models lagged over an additional decade.[28] Similarly, a culture system that recapitulates the human intestinal epithelium and enables the culture of important pathogenic human enteric viruses such as human noroviruses (HuNoVs) was developed only recently after decades of unsuccessful attempts.[29]

In alternative to disease reproduction, implications can be made through linkage/association. For TGV, several observations support the hypothesis of its linkage to trout granulomatosis: (i) the detection of TGV RNA (by RT-PCR) consistently correlated with clinical and pathological signs, whereas apparently healthy fish scored positive only infrequently. These few latter cases likely represented initial/subclinical disease events in affected farms and were never found in disease-free (Italian) farms. (ii) The spatial co-localization of TGV RNA (detected by FISH) with the hepatic lesions. (iii) The presence of electron-dense, coronavirus-like particles in granulomas (iv) The inability to detect or culture bacterial, fungi, or parasitic agents in diseased liver tissues.

Moreover, TGV's liver distribution and load correlated with disease appearance. In this respect, the presence of TGV in a few healthy fish and the detection of TGV RNA in non-granulomatotic tissues other than the liver are anticipated as such phenomena were described for additional viral pathogens. For example, in Atlantic salmon farms affected by the piscine myocarditis virus (*totivirus* genera), which causes the cardiomyopathy syndrome (CMS), apparently healthy Atlantic salmons were detected with the virus.[30] Moreover, RNA trasncripts of the piscine myocarditis virus were detected in spleen samples at rates that exceed those observed in the heart—the target organ of this virus.[30] Likewise, while the tissue distribution and load of piscine reovirus (PRV), the causative agent of heart and skeletal muscle inflammation (HSMI) in salmonids, are correlated with disease in infected Atlantic salmon, the virus is also detected in various organs and even in healthy and wild fish.[31] In mammals, the canine distemper virus is detectable in unaffected sites such as the urinary, gastric, and enteric mucosa and even in the skin, frequently in quantities that prevail over those found in the primary target organs—the brain and the respiratory tract.[32,33]

Within the assembled TGV genome, ORF1b shows significantly higher homology to other piscine nidoviruses than the predicted structural proteins. The spherical morphology of virions detected by electron microscopy (EM) in trout granulomas differs from that of other bafiniviruses, which predominantly appear rod shaped. Whether the differences between (one or more) TGV structural proteins and related bafiniviruses are leading to differences in virion morphology remains to be studied. Of note, several nidoviruses are pleomorphic, having virions with different morphological features. Examples include the Chinook salmon bafinivirus (spherical and bacillary virions)[17], green tree python nidovirus (rod and kidney shapes)[34], and ball python nidovirus (spherical and bacillary virions).[35]

A remarkable feature of TGV infection is the ensuing granulomatous disease, which is otherwise commonly associated with bacterial, mycotic, or parasitic infections. Nonetheless, granulomatous diseases are described for two (mammalian) nidoviruses: the ferret coronavirus, which occasionally mutates to ferret systemic coronavirus (FRSCV) that causes multisystemic granulomatous lesions in ferrets,[10] and the feline coronavirus (FCoV) that seldom causes feline infectious peritonitis (FIP).[11] Key features of these diseases are granulomatous/pyogranulomatous lesions in internal organs.[10,11] For FRSCV and FCoV, only a minority of infected animals develop a granulomatous disease.[36] This scenario resembles TGV infection in trout, where only 4%–7% of the individuals are macroscopically positive. The underlying mechanisms responsible for granuloma formation are largely unknown. Still, as demonstrated for FIP, they may include an immunologic component where B and T cell depletion and cytokine regulation generally accompany the clinical disease.[37,38] The fact that chronicity (aging lesions) in the morbid fish is proportionally correlated with the severity of the disease further supports progressive and complex pathogenesis.

Viruses may have a narrow or a broad host range. Whether TGV will expand within the rainbow trout population, spread to other localities, and potentially infect other species is of interest. Indeed, the case of

disease spread is well documented in viruses affecting lower vertebrates, which are often characterized by the wide host range. Infectious pancreatic necrosis virus (IPNV; Aquabirnavirus) was initially described (in the 1960s) as a pathogen of juvenile salmonids but soon was identified in a wide variety of fish, both freshwater and marine species.[39] Similarly, until the mid-1980s, IHNV (*Novirhabdovirus*) was considered a disease affecting mainly rainbow trout in continental Europe but during the following years has spread to a large range of free-living marine fish species throughout the northern hemisphere.[40] A wide host range has also been documented for piscine nidoviruses. The recently described bafinivirus of the Atlantic salmon was also identified in diseased goldfish.[17] These examples highlight the need to further study TGV host range.

In summary, the present study describes a new disease in the rainbow trout—a chronic hepatic disease characterized by granulomatotic lesions in the liver—and the identification of a novel nidovirus—TGV—which is associated with the disease. This study opens the way for new investigations, including TGV's host range, transmission routes, prevalence, and detailed clinical characteristics.

Limitations of the study

The inability to culture the virus did not allow us to fulfill Koch's postulates. It is also a significant obstacle in studying virus-host interactions and pathogenesis. It remains a challenge for future research.

STAR★METHODS

Detailed methods are provided in the online version of this paper and include the following:

- KEY RESOURCES TABLE
- RESOURCE AVAILABILITY
  - Lead contact
  - Materials availability
  - Data and code availability
- EXPERIMENTAL MODEL AND SUBJECT DETAILS
  - Animal studies
  - Cell lines and primary cultures
- METHOD DETAILS
  - Collection of specimens, and laboratory screening for known pathogens
  - Light and electron microscopy analyses
  - Cell lines and infection assays
  - Sample preparation for metagenomics
  - Next-generation sequencing and metagenomic pipeline
  - Amplification of viral sequences by RT-PCR and Sanger sequencing
  - Quantitative assays of viral transcripts
  - Nuclease sensitivity assays
  - Fluorescence *in situ* hybridization (FISH)
  - Ethics statement
- QUANTIFICATION AND STATISTICAL ANALYSIS

SUPPLEMENTAL INFORMATION

Supplemental information can be found online at https://doi.org/10.1016/j.isci.2023.106370.

ACKNOWLEDGMENTS

This work was supported by a U.S.-Israel Bi-National Agricultural Research and Development Fund grant (BARD IS-4903-16C) and by Israel Science Foundation grants (470/17 and 1952/22).

AUTHOR CONTRIBUTIONS

Conceptualization, As.B., Er.B., A.E., and S.K.; Methodology, A.F., S.W., K.L., A.H., Ar.B., and E.R.; Investigation, A.F., A.H., As.B., A.E., and S.K.; Visualization, Ed.B., Ar.B., E.R., M.O., M.G., As.B., A.E., and S.K. Writing–Original Draft, As.B., Er.B., A.E., and S.K.; Writing–revised manuscript, As.B., Er.B., A.E., I.S., and S.K. Supervision, A.E.

DECLARATION OF INTERESTS

The authors declare no competing interests.

Received: October 11, 2022
Revised: January 12, 2023
Accepted: March 6, 2023
Published: March 11, 2023

REFERENCES

1. Nielsen, R., Asche, F., and Nielsen, M. (2016). Restructuring European freshwater aquaculture from family-owned to large-scale firms–lessons from Danish aquaculture. Aquac. Res. *47*, 3852–3866.

2. Bergmann, S., Fichtner, D., Riebe, R., and Castric, J. (2008). First isolation and identification of sleeping disease virus (SDV) in Germany. Bull. Eur. Assoc. Fish Pathol. *28*, 148–156.

3. Olsen, A.B., Hjortaas, M., Tengs, T., Hellberg, H., and Johansen, R. (2015). First description of a new disease in rainbow trout (Oncorhynchus mykiss (Walbaum)) similar to heart and skeletal muscle inflammation (HSMI) and detection of a gene sequence related to piscine orthoreovirus (PRV). PLoS One *10*, e0131638. https://doi.org/10.1371/journal.pone.0131638.

4. Amend, D.F., Yasutake, W.T., and Mead, R.W. (1969). A hematopoietic virus disease of rainbow trout and sockeye salmon. Trans. Am. Fish. Soc. *98*, 796–804.

5. Jensen, M.H. (1965). Research on the virus of Egtved disease. Ann. N. Y. Acad. Sci. *126*, 422–426. https://doi.org/10.1111/j.1749-6632.1965.tb14292.x.

6. Gustafson, L.L., Ellis, S.K., Beattie, M.J., Chang, B.D., Dickey, D.A., Robinson, T.L., Marenghi, F.P., Moffett, P.J., and Page, F.H. (2007). Hydrographics and the timing of infectious salmon anemia outbreaks among Atlantic salmon (Salmo salar L.) farms in the Quoddy region of Maine, USA and New Brunswick, Canada. Prev. Vet. Med. *78*, 35–56.

7. McAllister, P.E., and Bebak, J. (1997). Infectious pancreatic necrosis virus in the environment: relationship to effluent from aquaculture facilities. J. Fish. Dis. *20*, 201–207.

8. Salama, N., and Murray, A. (2011). Farm size as a factor in hydrodynamic transmission of pathogens in aquaculture fish production. Aquac. Environ. Interact. *2*, 61–74.

9. Viljugrein, H., Staalstrøm, A., Molvaelr, J., Urke, H.A., and Jansen, P.A. (2009). Integration of hydrodynamics into a statistical model on the spread of pancreas disease (PD) in salmon farming. Dis. Aquat. Organ. *88*, 35–44.

10. Doria-Torra, G., Vidaña, B., Ramis, A., Amarilla, S.P., and Martínez, J. (2016). Coronavirus infection in ferrets: antigen distribution and inflammatory response. Vet. Pathol. *53*, 1180–1186. https://doi.org/10.1177/0300985816634809.

11. Kipar, A., and Meli, M.L. (2014). Feline infectious peritonitis: still an enigma? Vet. Pathol. *51*, 505–526. https://doi.org/10.1177/0300985814522077.

12. Batts, W.N., Goodwin, A.E., and Winton, J.R. (2012). Genetic analysis of a novel nidovirus from fathead minnows. J. Gen. Virol. *93*, 1247–1252. https://doi.org/10.1099/vir.0.041210-0.

13. Schütze, H., Ulferts, R., Schelle, B., Bayer, S., Granzow, H., Hoffmann, B., Mettenleiter, T.C., and Ziebuhr, J. (2006). Characterization of White bream virus reveals a novel genetic cluster of nidoviruses. J. Virol. *80*, 11598–11609. https://doi.org/10.1128/JVI.01758-06.

14. King, A.M., Lefkowitz, E., Adams, M.J., and Carstens, E.B. (2011). Virus Taxonomy: Ninth Report of the International Committee on Taxonomy of Viruses (Elsevier).

15. Nga, P.T., Parquet, M.D.C., Lauber, C., Parida, M., Nabeshima, T., Yu, F., Thuy, N.T., Inoue, S., Ito, T., Okamoto, K., et al. (2011). Discovery of the first insect nidovirus, a missing evolutionary link in the emergence of the largest RNA virus genomes. PLoS Pathog. *7*, e1002215. https://doi.org/10.1371/journal.ppat.1002215.

16. Katoh, K., Rozewicki, J., and Yamada, K.D. (2019). MAFFT online service: multiple sequence alignment, interactive sequence choice and visualization. Brief. Bioinform. *20*, 1160–1166.

17. Cano, I., Stone, D., Savage, J., Wood, G., Mulhearn, B., Gray, J., Stinton, N., Ross, S., Bonar, M., Taylor, N.G.H., et al. (2020). Isolation of a Chinook salmon bafinivirus (CSBV) in imported goldfish Carassius auratus L. In the United Kingdom and evaluation of its virulence in resident fish species. Viruses *12*, 578. https://doi.org/10.3390/v12050578.

18. Guindon, S., Dufayard, J.F., Lefort, V., Anisimova, M., Hordijk, W., and Gascuel, O. (2010). New algorithms and methods to estimate maximum-likelihood phylogenies: assessing the performance of PhyML 3.0. Syst. Biol. *59*, 307–321. https://doi.org/10.1093/sysbio/syq010.

19. Ulferts, R., Mettenleiter, T.C., and Ziebuhr, J. (2011). Characterization of Bafinivirus main protease autoprocessing activities. J. Virol. *85*, 1348–1359. https://doi.org/10.1128/JVI.01716-10.

20. Marchler-Bauer, A., and Bryant, S.H. (2004). CD-Search: protein domain annotations on the fly. Nucleic Acids Res. *32*, W327–W331. https://doi.org/10.1093/nar/gkh454.

21. Fehr, A.R., and Perlman, S. (2015). Coronaviruses: an overview of their replication and pathogenesis. Methods Mol. Biol. *1282*, 1–23. https://doi.org/10.1007/978-1-4939-2438-7_1.

22. Teufel, F., Almagro Armenteros, J.J., Johansen, A.R., Gíslason, M.H., Pihl, S.I., Tsirigos, K.D., Winther, O., Brunak, S., von Heijne, G., and Nielsen, H. (2022). SignalP 6.0 predicts all five types of signal peptides using protein language models. Nat. Biotechnol. *40*, 1023–1025. https://doi.org/10.1038/s41587-021-01156-3.

23. Krogh, A., Larsson, B., von Heijne, G., and Sonnhammer, E.L. (2001). Predicting transmembrane protein topology with a hidden Markov model: application to complete genomes. J. Mol. Biol. *305*, 567–580. https://doi.org/10.1006/jmbi.2000.4315.

24. Sonnhammer, E.L., von Heijne, G., and Krogh, A. (1998). A hidden Markov model for predicting transmembrane helices in protein sequences. Proc. Int. Conf. Intell. Syst. Mol. Biol. *6*, 175–182.

25. Howley, P.M., and Knipe, D.M. (2020). Fields Virology: Emerging Viruses (Lippincott Williams & Wilkins).

26. Sola, I., Almazán, F., Zúñiga, S., and Enjuanes, L. (2015). Continuous and discontinuous RNA synthesis in coronaviruses. Annu. Rev. Virol. *2*, 265–288. https://doi.org/10.1146/annurev-virology-100114-055218.

27. Gallo, R.C., and Montagnier, L. (2003). The discovery of HIV as the cause of AIDSN. Engl. J. Med. *349*, 2283–2285.

28. O'Brien, S.J., and Goedert, J.J. (1996). HIV causes AIDS: Koch's postulates fulfilled. Curr. Opin. Immunol. *8*, 613–618. https://doi.org/10.1016/s0952-7915(96)80075-6.

29. Ettayebi, K., Crawford, S.E., Murakami, K., Broughman, J.R., Karandikar, U., Tenge, V.R., Neill, F.H., Blutt, S.E., Zeng, X.L., Qu, L., et al. (2016). Replication of human noroviruses in stem cell-derived human enteroids. Science *353*, 1387–1393. https://doi.org/10.1126/science.aaf5211.

30. Garseth, Å.H., Fritsvold, C., Svendsen, J.C., Bang Jensen, B., and Mikalsen, A.B. (2018). Cardiomyopathy syndrome in Atlantic salmon Salmo salar L.: a review of the current

state of knowledge. J. Fish. Dis. *41*, 11–26. https://doi.org/10.1111/jfd.12735.

31. Palacios, G., Lovoll, M., Tengs, T., Hornig, M., Hutchison, S., Hui, J., Kongtorp, R.T., Savji, N., Bussetti, A.V., Solovyov, A., et al. (2010). Heart and skeletal muscle inflammation of farmed salmon is associated with infection with a novel reovirus. PLoS One *5*, e11487. https://doi.org/10.1371/journal.pone.0011487.

32. Garcia, P.A.T., Cartoceti, A., Affolter, V.K., Jackson, K., Keel, M.K., Agnew, D., Cooley, T., Melotti, J., Fitzgerald, S.D., and Pesavento, P.A. (2022). Distribution of canine distemper virus and nectin-4 in raccoon (Procyon lotor) skin. Vet. Pathol. *59*, 782–786. https://doi.org/10.1177/03009858221102598.

33. Kubo, T., Kagawa, Y., Taniyama, H., and Hasegawa, A. (2007). Distribution of inclusion bodies in tissues from 100 dogs infected with canine distemper virus. J. Vet. Med. Sci. *69*, 527–529. https://doi.org/10.1292/jvms.69.527.

34. Dervas, E., Hepojoki, J., Laimbacher, A., Romero-Palomo, F., Jelinek, C., Keller, S., Smura, T., Hepojoki, S., Kipar, A., and Hetzel, U. (2017). Nidovirus-associated proliferative pneumonia in the green tree Python (Morelia viridis). J. Virol. *91*, e00718-17. https://doi.org/10.1128/JVI.00718-17.

35. Stenglein, M.D., Jacobson, E.R., Wozniak, E.J., Wellehan, J.F.X., Kincaid, A., Gordon, M., Porter, B.F., Baumgartner, W., Stahl, S., Kelley, K., et al. (2014). Ball python nidovirus: a candidate etiologic agent for severe respiratory disease in Python regius. mBio *5*, e01484-14. https://doi.org/10.1128/mBio.01484-14.

36. Jaimes, J.A., and Whittaker, G.R. (2018). Feline coronavirus: insights into viral pathogenesis based on the spike protein structure and function. Virology *517*, 108–121. https://doi.org/10.1016/j.virol.2017.12.027.

37. Malbon, A.J., Fonfara, S., Meli, M.L., Hahn, S., Egberink, H., and Kipar, A. (2019). Feline infectious peritonitis as a systemic inflammatory disease: contribution of liver and heart to the pathogenesis. Viruses *11*, 1144. https://doi.org/10.3390/v11121144.

38. Malbon, A.J., Meli, M.L., Barker, E.N., Davidson, A.D., Tasker, S., and Kipar, A. (2019). Inflammatory mediators in the mesenteric lymph nodes, site of a possible intermediate phase in the immune response to feline coronavirus and the pathogenesis of feline infectious peritonitis? J. Comp. Pathol. *166*, 69–86. https://doi.org/10.1016/j.jcpa.2018.11.001.

39. Bandín, I., and Dopazo, C.P. (2011). Host range, host specificity and hypothesized host shift events among viruses of lower vertebrates. Vet. Res. *42*, 67. https://doi.org/10.1186/1297-9716-42-67.

40. Breyta, R., Brito, I., Ferguson, P., Kurath, G., Naish, K.A., Purcell, M.K., Wargo, A.R., and LaDeau, S. (2017). Transmission routes maintaining a viral pathogen of steelhead trout within a complex multi-host assemblage. Ecol. Evol. *7*, 8187–8200.

41. Scotto-Lavino, E., Du, G., and Frohman, M.A. (2006). 3′ end cDNA amplification using classic RACE. Nat. Protoc. *1*, 2742–2745. https://doi.org/10.1038/nprot.2006.481.

42. Kim, D., Pertea, G., Trapnell, C., Pimentel, H., Kelley, R., and Salzberg, S.L. (2013). TopHat2: accurate alignment of transcriptomes in the presence of insertions, deletions and gene fusions. Genome Biol. *14*, R36. https://doi.org/10.1186/gb-2013-14-4-r36.

43. Buchfink, B., Xie, C., and Huson, D.H. (2015). Fast and sensitive protein alignment using DIAMOND. Nat. Methods *12*, 59–60. https://doi.org/10.1038/nmeth.3176.

44. Li, D., Liu, C.M., Luo, R., Sadakane, K., and Lam, T.W. (2015). MEGAHIT: an ultra-fast single-node solution for large and complex metagenomics assembly via succinct de Bruijn graph. Bioinformatics *31*, 1674–1676. https://doi.org/10.1093/bioinformatics/btv033.

STAR★METHODS

KEY RESOURCES TABLE

REAGENT or RESOURCE	SOURCE	IDENTIFIER
Chemicals, peptides, and recombinant proteins		
RiboEx LS	GeneAll Biotechnology	# 302-001
Critical commercial assays		
Direct-zol RNA Miniprep Kit	Zymo Research	#R2050
RiboMinus™ Eukaryote Kit for RNA-Seq	Thermo Fisher Scientific	# A1083708
NEXTFLEX® Rapid Directional RNA-Seq Kit	Perkin Elmer	# NOVA-5130
NEBNext UltraII Directional RNA Library Prep Kit	New England BioLabs	#E7530
QIAamp Viral RNA Mini Kit	Qiagen	# 52906
XLT 1-Step RT-PCR Kit	Quanta bio	# 95143
qScript XLT 1-Step RT-qPCR ToughMix ROX kit	Quanta bio	# 95133
SuperScript™ III First-Strand Synthesis System	Thermo Fisher Scientific	# 18080051
PCRBIO Verifi Polymerase	PCR Biosystems	# PB10.42
MEGAquick-spin™ Plus Total Fragment DNA Purification Kit	iNtRON	# 17290
RiboMAX Large Scale RNA Production System	Promega	#P1300
Deposited data		
TGV 1b partial ORF	This manuscript	Genbank: NM_OM397548
TGV complete genome	This manuscript	Genbank: NC_OP060531
Rainbow trout samples used for metagenomics RNA-seq	This manuscript	BioSample: SAMN29837949
Biological data for metagenomics RNA-seq of Rainbow trout samples	This manuscript	BioProject: PRJNA860318
Metagenomic RNA-seq data of Rainbow trout samples	This manuscript	SRA: SRR20324708
Experimental models: Cell lines		
Common bluegill: CHSE-214	ATCC	CRL-1681
Common bluegill: BF-2	ATCC	CCL-91
Fathead Minnow: EPC	ATCC	CRL-2872
Rainbow Trout: SOB-15	ATCC	CRL-2301
Rainbow Trout: RTgill-W1	ATCC	CRL-2523
Rainbow Trout: RTG-2	ATCC	CCL-55
Rainbow Trout: RTH-149	ATCC	CRL-1710
Atlantic Salmon: ASK	ATCC	CRL-2747
Sockeye Salmon: SSE5	ECACC	95122021
Oligonucleotides		
PCR Primers and Probe devised for this study, see Table S1	This manuscript	N/A

(*Continued on next page*)

Continued

REAGENT or RESOURCE	SOURCE	IDENTIFIER
QT: ccagtgagcagagtgacgagga ctcgagctcaagcttttttttttttttt	Scotto-Lavino et al.[41]	N/A
QO: ccagtgagcagagtgacg	Scotto-Lavino et al.[41]	N/A
QI: gaggactcgagctcaagc	Scotto-Lavino et al.[41]	N/A
Stellaris RNA FISH probes TGV specific, se Table S2	This manuscript	N/A
Software and algorithms		
FastQC	Babraham Bioinformatics	https://www.bioinformatics.babraham.ac.uk/projects/fastqc/
FASTX	Hannon lab CSHL	http://hannonlab.cshl.edu/fastx_toolkit/index.html
Tophat2 v. 2.1	Kim et al.[42]	https://ccb.jhu.edu/software/tophat/index.shtml
DIAMOND	Buchfink et al.[43]	https://uni-tuebingen.de/en/fakultaeten/mathematisch-naturwissenschaftliche-fakultaet/fachbereiche/informatik/lehrstuehle/algorithms-in-bioinformatics/software/diamond/
SignalP	Fehr and Perlman[21], Teufel et al.[22]	https://services.healthtech.dtu.dk/service.php?SignalP
Mafft	Katoh et al.[16]	https://mafft.cbrc.jp/alignment/server/
NCBI conserved domains algorithm	Marchler-Bauer and Bryant[20]	https://www.ncbi.nlm.nih.gov/Structure/cdd/wrpsb.cgi
TMHMM 2.0 algorithm	Krogh et al.[23], Sonnhammer et al.[24]	https://services.healthtech.dtu.dk/service.php?TMHMM-2.0
Geneious 9.1.8	Geneious	https://www.geneious.com
Megahit	Li et al.[44]	https://github.com/voutcn/megahit
Nikon NIS-Elements D imaging software	Nikon	https://www.microscope.healthcare.nikon.com/products/software/nis-elements/nis-elements-documentation
GraphPad Prism 5.0	GraphPad	https://www.graphpad.com/scientific-software/prism/
Other		
Supercut Microtome	Leica	Reichert-Jung 2050
Upright Microscope Nikon Eclipse CI-L	Nikon	https://www.microscope.healthcare.nikon.com/products/upright-microscopes/eclipse-ci-series
Inverted Microscope Nikon TE 2000-U	Nikon	https://www.microscopyu.com/museum/eclipse-te2000-inverted-microscope
Transmission Electron Microscope JEM-1400 Plus	Jeol	https://www.jeol.com/products/scientific/tem/JEM-1400Plus.php
Bioanalyzer 2100	Agilent Technologies	https://www.agilent.com/en/product/automated-electrophoresis/bioanalyzer-systems/bioanalyzer-instrument
HiSeq 2500	Illumina	https://emea.illumina.com/systems/sequencing-platforms/hiseq-2500.html
HiSeq XTen	Illumina	https://www.illumina.com/systems/sequencing-platforms/hiseq-x.html
StepOnePlus real-time PCR machine	Applied Biosystems	# 4376600

RESOURCE AVAILABILITY

Lead contact

Further information and requests for resources and reagents should be directed to and will be fulfilled by the lead contact, Sharon Karniely (sharonk@moag.gov.il).

Materials availability

This study did not generate new unique reagents.

Data and code availability

- Metagenomic RNA sequencing data have been deposited at SRA database and are publicly available as of the date of publication. Assembled TGV 1b partial ORF and TGV complete genomic sequences have been deposited in NCBI Genbank and are publicly available as of the date of publication. Accession numbers are listed in the key resources table. Microscopy data reported in this paper will be shared by the lead contact upon request.
- This paper does not report original code.
- Any additional information required to reanalyze the data reported in this paper is available from the lead contact upon request.

EXPERIMENTAL MODEL AND SUBJECT DETAILS

Animal studies

This study did not involve experimentation with animals. Farmed Rainbow trout (*Oncorhynchus mykiss*) all female stocks, weighing 250 to 350g, were collected for inspection by the national veterinary services. Necroscopic, parasitological, bacteriological examinations and molecular analysis were performed as described below.

Cell lines and primary cultures

CHSE-214 (ATCC CRL-1681) derived from Common bluegill (*Lepomis macrochirus*) (not Chinook salmon (*Oncorhynchus tshawytscha*) as originally reported), Bluegill fry-2 (BF-2; ATCC CCL-91) derived from the Common bluegill (*Lepomis macrochirus*) and the epithelioma papillosum of carp (EPC; ATCC CRL-2872) originally deposited as Carp (*Cyprinus carpio*) and subsequently found to be Fathead Minnow (*Pimephales promelas*) through cytochrome c oxidase subunit I testing at ATCC. Salmonid fish cell lines included the rainbow trout (*Oncorhynchus mykiss*) liver epithelium SOB-15 (ATCC CRL-2301), rainbow trout RTgill-W1 (ATCC CRL-2523), rainbow trout gonad 2 (RTG-2, ATCC CCL-55), and rainbow trout hepatoma (RTH-149, ATCC CRL-1710), the fish Sockeye Salmon (*Oncorynchus nerka*) embryo (SSE5 , ECACC 95122021) cell line and the Atlantic Salmon (*Salmo salar*) Kidney (ASK, ATCC CRL-2747) cell line.

Primary cells were prepared from minced rainbow trout tissues (liver, tongue, skin, and brain) by trypsinization and subculturing.

Primary cells and cell lines were cultured in L-15 medium (Gibco) supplemented with 10% Fetal Bovine Serum (FBS, Gibco), 20mM L-Glutamine (Biological industries), 100 units/ml Penicillin G Sodium Salt (Biological industries), 0.1 mg/mL Streptomycin Sulfate (Biological industries) and 0.25 µg/mL Amphotericin B (Biological industries) and maintained at 18°C.

METHOD DETAILS

Collection of specimens, and laboratory screening for known pathogens

A total of 50 rainbow trout, each weighing 250 to 350g, were collected during February-June 2018 from commercial stocks while being graded for marketing. The sampled fish showed decreased swimming movements and gathered at the lower end of the raceway, characteristic of general weakness. Controls consisted of 50 (apparently) healthy fish of similar size. All fish were subjected to complete necroscopic, parasitological, and bacteriological examinations. The histopathological assessment included section staining with hematoxylin and eosin, Brown and Brenn, Ziehl–Neelsen, Warthin–Starry, Giemsa, and Grocott-Gomori methenamine silver stains. For the detection of known viruses capable of infecting salmonids [piscine orthoreovirus (PRV), infectious salmon anaemia virus (ISAV), salmonid alphavirus (SAV), piscine myocarditis virus (PMCV), viral haemorrhagic septicaemia virus (VHSV), infectious hematopoietic necrosis virus (IHNV), and infectious pancreatic necrosis virus (IPNV)], 6 pools of diseased fish (3 fish per pool) were randomly selected and screened by reverse transcription polymerase chain reaction (RT-PCR) amplification using primers and probes as described elsewhere (OIE Aquatic Manual; https://www.oie.int/en/what-we-do/standards/codes-and-manuals/).

Light and electron microscopy analyses

For the histological study, samples (from apparently infected livers) were fixed in 10% neutral buffered formalin, embedded in paraffin (Paraplast Plus; Diapath), cut by microtome (Reichert-Jung 2050) into serial 5-μm sections, stained with hematoxylin and eosin (H&E), and examined under a light microscope (Nikon Eclipse CI-L). Images were acquired by a Nikon digital light system.

For transmission electron microscopy (TEM), liver biopsies (approx. 2 mm) were fixed in a 1.5% glutaraldehyde plus 1.5% formaldehyde in 0.1 M sodium cacodylate (pH 7.2) solution for 2 h and then overnight at 4°C ,rinsed three times in 0.1 M sodium cacodylate (pH 7.2) solution. Samples were postfixed in 1% OsO4 in 0.1 M sodium cacodylate (pH 7.2) solution and dehydrated with increasing ethanol concentrations. The samples were washed twice with 100% propylene oxide and treated with propylene oxide-Epon (3:1) for 30 min, followed by propylene oxide-Epon (1:1) for 15 min and propylene oxide-Epon (1:3) for 15 min. Finally, the samples were embedded in 100% Epon and left overnight. Thin sections (70 to 90 nm) were placed on formvar-coated copper grids and stained with uranyl acetate, followed by lead citrate, according to the Reynolds method (Reynolds, 1963). All micrographs were taken with a JEOL JEM-1400 Plus electron microscope operating at 100 kV (Electron Microscopy [EM] Unit, Faculty of Medicine, Hadassah Medical School at the Hebrew University of Jerusalem, Israel).

Cell lines and infection assays

As routine bacteriological and parasitological tests failed to identify a common denominator for the disease, we decided to attempt virus isolation in line with procedures described in Commission Decision 2001/183/EC (http://eurlex.europa.eu/LexUriServ/LexUriServ.do?uri=OJ:L:2001:067:0065:0076:EN:PDF). Tissue homogenates (pools of livers, brains, spleens, and kidneys) from diseased fish were prepared, and 500 μl of 0.22 nm filtrates were inoculated on the cell lines and primary cultures described above (*Cell lines and primary cultures*). Cells were inoculated with homogenates (40 min at 18°C), and cultures were then washed with PBS, supplemented with L-15 medium (2% FCS), and incubated at 18°C. Cultures were observed for 14 days for cytopathic effects (CPE) and monitored for additional two passages.

Sample preparation for metagenomics

In parallel with our attempts at virus isolation, we employed next-generation sequencing to identify possible causative agent(s) of the disease. The liver was chosen as the organ of relevance as it is the site of cardinal macroscopic and microscopic changes (hepatocyte degeneration, multifocal necrotic lesions, and white plaque formation; see results). Liver biopsies from a diseased or a healthy fish were homogenized manually and lysed in RiboEx LS Total RNA purification solution (GeneAll Biotechnology, Seoul, Korea). Total RNA was extracted using Direct-zol RNA Miniprep Kit (Zymo Research, CA) and included an on-column DNaseI treatment to remove genomic DNA. RNA purity was determined by spectrophotometric readings 260/280 nm and 260/230 nm absorption ratios using Nanodrop ND-1000 (PeqLab, Erlangen, Germany). RNA integrity was verified via RNA Integrity Number (RIN) measured by capillary electrophoresis measurements using the Bioanalyzer 2100 (Agilent Technologies).

Next-generation sequencing and metagenomic pipeline

1 μg of Total RNA was depleted of ribosomal RNA using RiboMinus™ Eukaryote Kit for RNA-Seq (Thermo Fisher Scientific), and sequencing libraries were prepared using NextFlex Rapid Directional qRNA Seq kit (Perkin-Elmer). The libraries were quantified, pooled in equimolar concentration, and sequenced on the next-generation sequencing platform Illumina HiSeq 2500 (Illumina, Genome Research Core Lab University of Illinois, Chicago, USA), producing 12.4 M and 11.2 M 2 × 150 -nucleotide paired-end reads for the diseased and healthy sample, respectively. For quality assessment and trimming, the raw reads were screened with FastQC (http://www.bioinformatics.babraham.ac.uk/projects/fastqc/) and the FASTX toolkit (http://hannonlab.cshl.edu/fastx_toolkit/index.html). Clean reads were mapped to the reference genome of rainbow trout (GCF_002163495) using Tophat2 software v. 2.1 (Kim et al., 2013). Unaligned reads were used as a query term for a search of the NCBI non-redundant (nr) protein database, carried out with the DIAMOND software.[43] An additional RNA-seq was performed on a liver sample pre-screened for the high abundance of TGV-specific replicase sequences. 100 ng of total RNA (not depleted of rRNA) were used for library preparation using Illumina-compatible NEBNext UltraII Directional RNA Library Prep Kit (New England BioLabs), according to the manufacturer's instructions. Sequencing was carried out on HiSeq XTen for 150 cycles, following the manufacturer's instructions (Illumina, producing 30 million

2x150 paired-end. Library preparation and sequencing of this sample were performed at Genotypic Technology Pvt. Ltd., Bangalore, India.

Amplification of viral sequences by RT-PCR and Sanger sequencing

Samples from the livers of diseased and healthy fish were homogenized, and total RNA was extracted using QIAamp Viral RNA Mini Kit (Qiagen) according to the manufacturer's instructions. PCR amplification of viral sequences was performed by one-step RT-PCR using primer sets designed to tile across the available sequences, targeting reads suspected to be part of the viral genome. Reactions were conducted in a final volume of 25 μl with qScript XLT 1-Step RT-PCR Kit (Quanta bio) according to the manufacturer's instructions. The cycling parameters were as follows: reverse transcription at 48°C/40 min followed by 94°C/3 min and PCR: 40 cycles of 94°C/20 s, 58°C/30 s, and 72°C/1 min per expected kb. Alternatively, a two-step approach was used where cDNA was produced using SuperScript™ III First-Strand Synthesis System (Thermo Fisher Scientific) with oligo-dT priming according to the manufacturer's instructions followed by PCR with PCRBIO Verifi Polymerase (PCR Biosystems LTD).

PCR products were visualized by gel electrophoresis. All PCR products of approximately the right size were purified using MEGAquick-spin™ Plus Total Fragment DNA Purification Kit (iNtRON). Sanger sequencing was performed at HyLab laboratories, Rehovot, Israel, and Macrogen, Amsterdam, the Netherlands. Obtained sequences were assembled using the Geneious 9.1.8 software (https://www.geneious.com) and subjected to BlastX analysis blasted against GenBank Non-redundant protein sequences (nr) database. In addition, the Megahit program was also used for assembling the obtained reads, which were used for homology search against the NR database by the DIAMOND software.[43]

Negative controls consisted of rainbow trout liver biopsies of 10 healthy rainbow trout and samples originating from two unrelated rainbow trout farms (located in the North-West and the center of Italy) without the observed disease.

The 3′ end of the TGV genome was determined using 3′ RACE as previously described[41] with minor modifications. 5 μg of total RNA were taken for a first strand cDNA synthesis reaction (20 μl) with SuperScript III reverse transcriptase (Thermo Scientific) according to the manufacturer's instructions using 2.5 μM of the oligonucleotide(dT)-tailed primer QT [5′ ccagtgagcagagtgacgaggactcgagctcaagcttttttttttttttttt 3′,[41]]. Reverse transcription was performed at 50°C/50 min, followed by inactivation at 85°C/5 min and digestion with 2 Units RNase H at 37°C/20 min. cDNA was diluted in 400 μl of Tris–EDTA buffer (10 mM Tris-HCl, pH 7.5/ 1 mM EDTA). 2 μl of diluted cDNA were used for first round PCR amplification in a final volume of 25 μl with PCRBIO Verifi Polymerase (PCR Biosystems LTD), 10 μM of TGV specific Spike 5-F1 forward primer (5′ tcgctggcatggatttcgtatc 3′) and QO reverse primer [5′ ccagtgagcagagtgacg 3′[41]]. One round of 95°C/3 min, 53°C/2 min, and 72°C/40 min was followed by 30 cycles of 95°C/15 s, 53°C/15s and 72°C/3 min and a final extension step of 72°C/15 min. Second round of PCR (35 cycles) was performed as above using 2 μl of first round PCR reaction as template and internal (nested) primers: Spike 5-F2 (5′ atccaactacctaccactggct 3′) and QI [5′ gaggactcgagctcaagc 3′[41]].

Quantitative assays of viral transcripts

Quantitative assays were established based on virus-specific sequences obtained from the high throughput sequencing. Relative Viral RNA loads of each specimen were assessed by reverse transcription quantitative (real-time) PCR (RT-qPCR) using the qScript XLT 1-Step RT-qPCR ToughMix ROX kit (QuantaBio). Primers and probes targeting TGV ORF1b and the rainbow trout 18S ribosomal RNA (rRNA) host reference gene (GenBank accession number AF308735) were designed using the Genious 9.1.8 software (https://www.geneious.com). We have used a duplex reaction for both targets using a FAM-labeled probe for TGV and a Hex-labeled probe for Trout 18S (Table S1). Reactions were performed according to the manufacturer's instructions using 400 nM primers and 100 nM probe. Amplifications were done in a StepOnePlus real-time PCR machine (ABI) with the following cycling parameters: 10 min at 50 °C (reverse transcription), 5 min at 95 °C (RT inactivation), 45 cycles of 94 °C /15 sec and 60 °C /30 sec. Relative viral RNA levels were determined by normalization to the host 18S rRNA using the $2^{-\Delta\Delta Ct}$ method using a healthy liver sample with the lowest TGV copies as reference. Samples having TGV Ct>38 were regarded as TGV negative, and the relative expression of TGV in these samples was arbitrarily given a value of one. To assess the absolute number of copies of viral RNA in samples, we calibrated Ct values to a measured amount of *in vitro* synthesized TGV 1b transcript. We amplified a 1,020 bp sequence within the TGV1b

coding region containing the 160 bp target RT-qPCR sequence and added the T7 promoter with the 5' end forward primer. This DNA amplicon was purified and was used as a template for *in vitro* transcription using the RiboMAX Large Scale RNA Production System (Promega). The resulting synthetic RNA was DNase-I treated (to eliminate the template), purified, and quantified using an RNA-specific Dye (AccuBlue, Biotium) and fluorimetry. RNA mass was converted to RNA copies using the calculated molecular weight of the TGV RNA transcript and used for building a calibration curve against Ct values obtained in RT-qPCR using serially diluted synthetic RNA. The detection limit was 11 copies (Ct=38).

Nuclease sensitivity assays

RNA was extracted from liver tissues as described above and resuspended in 300 µl of DNase buffer (10mMTris-HCl [pH 7.5], 2.5mM $MgCl_2$, and 0.5mM $CaCl_2$) and supplemented with either 2 µl of RNase A (10mg/ml, Thermo Scientific) or 2 µl DNase I (1U/ µl, Thermo Scientific). Samples were incubated for 30 min at 37°C; DNase I was then inactivated using 1uL 50mM EDTA and an incubation step of 10 min at 65°. RNA was cleaned up from enzymes using the easy spin Total RNA isolation kit (iNtRON Biotechnology, Korea), after which the RT-PCR reaction was performed as described above.

Fluorescence *in situ* hybridization (FISH)

To detect RNA of the novel virus, *in situ* hybridizations were performed with Stellaris RNA FISH probes (Biosearch Technologies, UK) and liver sections according to the manufacturer's instructions. The tissue samples were collected from euthanized fish and fixed in 10% neutral buffered formalin. Specimens were embedded in paraffin and serially sectioned (5 µm thick). Slides were deparaffinized by incubation in 100% xylene for 10 minutes and an additional 5 minutes of incubation in fresh xylene. Deparaffinized slides were immersed sequentially in 100% ethanol (twice) and 95% ethanol each for 10 minutes and then for 4 hours in 70% ethanol. Slides were then immersed in 1X PBS for 2-5 minutes and digested with molecular biology grade proteinase K (10 µg/ml in pre-warmed 1X PBS) for 20 minutes at 37 °C. After washing with Buffer A (10% (v/v) formamide in 2xSSC (0.3 M NaCl, 30 mM sodium citrate, pH 7.0)), sections were hybridized overnight at 37°C in a humidified chamber with FISH hybridization buffer (100 mg/mL dextran sulfate, 10% (v/v) formamide in 2xSSC) containing 125 nM custom-designed Stellaris RNA FISH probes targeting the identified viral sequence labelled with Quasar 570 or a non-targeting probe as control. Slides were then washed twice for 30 minutes with warm (37 °C) buffer A, followed by one wash with buffer B (2xSSC) and counterstained with Hoechst (1 µg/mL). Imaging was performed using a Nikon TE 2000-U widefield microscope with an X20 air or X60 oil-immersion objective and a DS-Qi2 camera using NIS-Elements D imaging software (Nikon).

Ethics statement

Samples were collected by fish health personnel authorized to investigate fish diseases as part of their regular disease diagnostic activity. No endangered or protected species were involved. This study meets all applicable standards for the ethics of research integrity.

QUANTIFICATION AND STATISTICAL ANALYSIS

Statistical analyses were performed using GraphPad 5.0 (Prism) software. Statistical details of experiments can be found in the figure legends. All the results are indicated as the geometric mean values with a confidence interval (CI) of 95 %. The statistical significance was determined by Mann-Whitney U test. Significant differences between data were indicated with *p-value < 0.05; **p-value < 0.01; ns, not significant.